Virology 538 (2019) 1–10

Contents lists available at ScienceDirect

Virology

journal homepage: www.elsevier.com/locate/virology

Replication of HIV-1 envelope protein cytoplasmic domain variants in permissive and restrictive cells

August O. Staubus, Ayna Alfadhli, Robin Lid Barklis, Eric Barklis*

Department of Molecular Microbiology and Immunology, Oregon Health and Sciences University, 3181 SW Sam Jackson Park Road, Portland, OR, 97239, USA

ARTICLE INFO

Keywords:
HIV-1
Replication
Envelope protein
Cytoplasmic tail

ABSTRACT

Wild type (WT) HIV-1 envelope (Env) protein cytoplasmic tails (CTs) appear to be composed of membrane-proximal, N-terminal unstructured regions, and three C-terminal amphipathic helices. Previous studies have shown that WT and CT-deleted (ΔCT) Env proteins are incorporated into virus particles via different mechanisms. WT Env proteins traffic to cell plasma membranes (PMs), are rapidly internalized, recycle to PMs, and are incorporated into virions in permissive and restrictive cells in a Gag matrix (MA) protein-dependent fashion. In contrast, previously described ΔCT proteins do not appear to be internalized after their arrival to PMs, and do not require MA, but are only incorporated into virions in permissive cell lines. We have analyzed a new set of HIV-1 CT variants with respect to their replication in permissive and restrictive cells. Our results provide novel details as to how CT elements regulate HIV-1 Env protein function.

1. Introduction

The pathways by which HIV-1 envelope (Env) proteins become incorporated into virions are complicated and incompletely elucidated (Checkley et al., 2011). They are cell type-dependent, and are affected by mutations in the HIV-1 Gag protein matrix (MA) and Env cytoplasmic tail (CT) domains (Checkley et al., 2011; Freed and Martin, 1995, 1996; Murakami and Freed, 2000a, 2000b; Tedbury et al., 2013, 2016; Yu et al., 1992; Wang et al., 1993; Dorfman et al., 1994; Reil et al., 1998; Bhatia et al., 2009; Bhakta et al., 2011; Alfadhli et al., 2016; Qi et al., 2013, 2015; Kirschman et al., 2018). Evidence indicates that full-length wild type (WT) HIV-1 Env proteins are translated and initially glycosylated at rough endoplasmic reticulum (RER) membranes to yield membrane-anchored 160 kDa glycoprotein precursor (gp160) proteins (Checkley et al., 2011). The gp160 monomers oligomerize in the ER, and traffic to the Golgi, where they acquire complex carbohydrates and are cleaved by furin or furin-like proteases to yield non-covalently associated surface (SU; gp120) and transmembrane (TM, gp41) proteins (Checkley et al., 2011; Pinter et al., 1989; Schawaller et al., 1989; Earl et al., 1990; Bernstein et al., 1994; Montefiori et al., 1988; Hallenberger et al., 1992). Trimers of associated gp120 and gp41 proteins then are delivered to cell plasma membranes (PMs), where they are subject to rapid endocytosis by virtue of YxxL AP-2 binding sites at the membrane proximal ends of CTs, and/or LL AP-1 binding sites at the CT C-termini (Qi et al., 2013, 2015; Kirschman et al., 2018; Ohno et al., 1997; Wyss et al., 2001). Internalized Env proteins either are shunted off to lysosomes for degradation, or return to PMs on recycling endosomes in a pathway that is dependent, in certain cell types, on the Rab11 coupling protein FIP1C (Qi et al., 2013, 2015; Kirschman et al., 2018). WT HIV-1 Env proteins, delivered to PMs in this fashion can be assembled into Gag lattices and, in this way, incorporated into virions.

In contrast to full-length WT Env proteins, HIV-1 Env proteins with CT deletions (ΔCT) that lack the YxxL AP-2 binding site appear to be delivered to cell PMs similarly to WT proteins, but are not internalized, and do not require HIV-1 MA proteins for incorporation into virions (Freed and Martin, 1995, 1996; Murakami and Freed, 2000a, 2000b; Reil et al., 1998; Qi et al., 2013, 2015; Kirschman et al., 2018; Mammano et al., 1995). Interestingly, the ability of ΔCT HIV-1 Env proteins to assemble into virions is cell type-dependent: human T cell lines such as Jurkat and CEM-SS cells are restrictive for ΔCT incorporation into virions, while MT-4 T cells, human embryonic kidney 293T (293T) cells, and human cervical cancer HeLa-derived cells are permissive for incorporation (Murakami and Freed, 2000a; Qi et al., 2013, 2015; Kirschman et al., 2018).

Recent studies have verified previous models for the structure of the HIV-1 CTs, showing a largely unstructured N-terminal membrane-proximal region, and three amphipathic helices referred to as lentivirus lytic peptides (LLP-2, LLP-3, and LLP-1 from N- to C-termini) that lie roughly parallel to membranes (Checkley et al., 2011; Murphy et al.,

* Corresponding author.
E-mail address: barklis@ohsu.edu (E. Barklis).

https://doi.org/10.1016/j.virol.2019.09.008
Received 1 July 2019; Received in revised form 13 September 2019; Accepted 17 September 2019
Available online 18 September 2019
0042-6822/

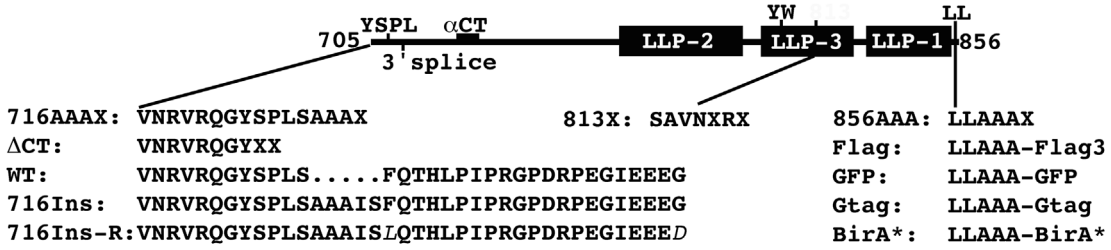

Fig. 1. Envelope CT variants. Shown is a diagram of the HIV-1 NL4-3 strain Env CT residues 705–756 with residues involved in AP2 binding (YSPL, residues 712–715), FIP1C binding (YW, residues 795-6), and AP1 binding (LL, residues 855-6) indicated. Also shown is the Rev third exon 3′ splice site (nt. 8369), the location (residues 727–732) of the Chessie 8 anti-CT antibody (αCT), and three dark bars indicative (from left to right) of the helical lentivirus lytic peptide 2 (residues 753–785), 3 (residues 790–823) and 1 (residues 827–856) regions. The WT sequence of residues 705–737 are given, as are the translation termination sequences of the ΔCT and 716AAAX variants. Relative to the WT sequence, the 716Ins variant carries an insertion of the residues AAAIS after residue 716, while the two mutated residues in the 716Ins revertant (716Ins-R) are depicted in italic font. The truncation mutant 813X stops after residue 813 as indicated, and 856AAA carries three additional alanine residues at the Env C-terminus. The Flag, GFP, Gtag, and BirA* variants include three alanine residues after Env residue 813 but respectively carry C-terminal three Flag epitopes (Flag), the GFP coding region (GFP), the cytoplasmic domain of the VSV G protein (Gtag), or the promiscuous bacterial biotin ligase (BirA*) coding region.

2017). Despite this information, major questions linger concerning how Env proteins are incorporated into virions, and what CT alterations are tolerated for replication in permissive or restrictive cell types. We have examined the effects of new CT truncations and insertions on HIV-1 replication, Env expression and Env localization. Our results reveal novel aspects of HIV-1 Env CT function and processing.

2. Results

2.1. Replication analysis of env protein truncation and small insertion variants

In addition to WT HIV-1 and the previously described ΔCT virus (Freed and Martin, 1995), we initially examined two HIV-1 Env CT truncation mutations, and two insertion variants. One of the truncation mutations, 716AAAX, terminates CT after Env codon 716, with a series of three alanine codons and a stop codon (Fig. 1). This locates to the N-terminal CT unstructured region (Murphy et al., 2017), just past the AP-2 YxxL binding site. The second truncation mutation, 813X, terminates CT translation immediately after Env codon 813 in LLP-3, eighteen residues downsteam from the YW motif that was shown to affect FIP1C binding (Fig. 1, Qi et al., 2013, 2015). The insertion mutations, 716Ins and 856AAA (Fig. 1), respectively carry a five codon insertion (AAAIS) after Env codon 716, or a three alanine codon insertion at the CT C-terminus. These were chosen to test whether the membrane-proximal unstructured region (Murphy et al., 2017) tolerates mutation, and whether a free C-terminus is critical for replication. For our investigations, mutations were incorporated into HIV-1 NL4-3 proviral constructs (Adachi et al., 1986), viruses were produced by transfection of permissive 293T cells, and normalized amounts of viruses were used to infect permissive (MT-4) and restrictive (CEM-SS) T cell lines (Murakami and Freed, 2000a; Qi et al., 2013, 2015; Kirschman et al., 2018). However, prior to undertaking infections, we monitored FIP1C levels in the 293T, MT-4, and CEM-SS cell lines, along with permissive (Murakami and Freed, 2000a; Qi et al., 2013, 2015; Kirschman et al., 2018) HeLa cells. As shown in Fig. 2, roughly equivalent FIP1C levels were observed in HeLa, 293T, and CEM-SS cells. In contrast, no FIP1C was detected in MT-4 cells, supporting the notion that different cellular factors are responsible for WT and/or ΔCT Env incorporation into virions in this cell line.

Our first set of infections included WT and ΔCT controls, along with the 716AAAX truncation mutant, and the 856AAA insertion mutant (Fig. 3A-B). As expected, WT HIV-1 replicated well in both permissive MT-4 and restrictive CEM-SS cells, while the ΔCT virus showed a slight replication delay in MT-4 cells (Fig. 3A), but was non-infectious in CEM-SS cells (Fig. 3B). The 856AAA variant replicated with WT kinetics in both cell lines, indicating that the addition of the three alanine

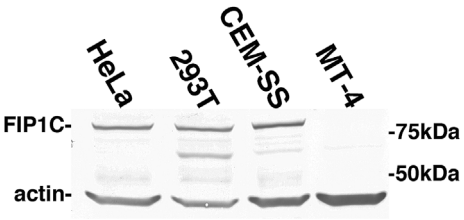

Fig. 2. FIP1C protein levels in different cell types. FIP1C and actin protein levels in HeLa, HEK293T (293T), CEM-SS, and MT-4 cells were determined after electrophoretic fractionation of cell lysate samples by successive immunoblot detection steps for FIP1C and actin proteins. The mobilities of 75kDa and 50 kDa marker proteins run in parallel are indicated. Note that replication of ΔCT HIV-1 is restricted in CEM-SS cells due to inefficient Env incorporation into virions, while HeLa, 293T, and MT-4 cells are permissive for assembly of ΔCT proteins into virus particles.

residues at the C-terminus of Env did not impair virus replication. In contrast, the 716AAAX truncation mutant virus was defective in both permissive and restrictive cell types (Fig. 3A-B).

In a subsequent infection experiment (Fig. 3C-D), WT and 716AAAX viruses again were tested, along with the 716Ins virus. Not surprisingly, the WT virus again replicated well in both MT-4 and CEM-SS cells, while the 716AAAX virus was defective. The 716Ins virus showed a different phenotype. In particular, 716Ins demonstrated a slight replication delay in MT-4 cells (Fig. 3C), but a 50 day delay in CEM-SS cells (Fig. 3D). To ascertain whether these late-replicating viruses might be revertants, they were collected, designated as putative revertant (716Ins-R) stocks, normalized to WT, 716Ins parental, and 813X truncation virus stocks, and used to infect new MT4 and CEM-SS cells (Fig. 4A-B). In these infections, 813X and parental 716Ins viruses showed similar phenotypes, with slightly delayed replication kinetics in MT-4 cells, and no replication in CEM-SS cells. However, the 716Ins-R stock replicated at the WT rate in MT-4 cells (Fig. 4A), and at only a slightly delayed rate in CEM-SS cells (Fig. 4B), strongly supporting the idea that the 716Ins-R stock contained revertant viruses.

To identify possible reversion mutations in 716Ins-R stock viruses, MA and Env regions from 716Ins-R-infected cells were amplified, cloned, and sequenced. Sequence analysis indicated no changes in MA, but two point mutations in Env, relative to the 716Ins virus: one changing Env codon 717 from F to L (ttt to ctt), and one changing Env codon 737 from G to D (ggt to gat; see Fig. 1). To test whether these mutations were sufficient to confer the 716Ins-R phenotype, the region containing these mutations was used to replace the analogous region in the 716Ins parent to yield a molecular clone designated 716Ins-R*. Next, 716Ins-R* viruses were produced and employed in infections in parallel with WT, ΔCT, and parental 716Ins viruses. As illustrated in

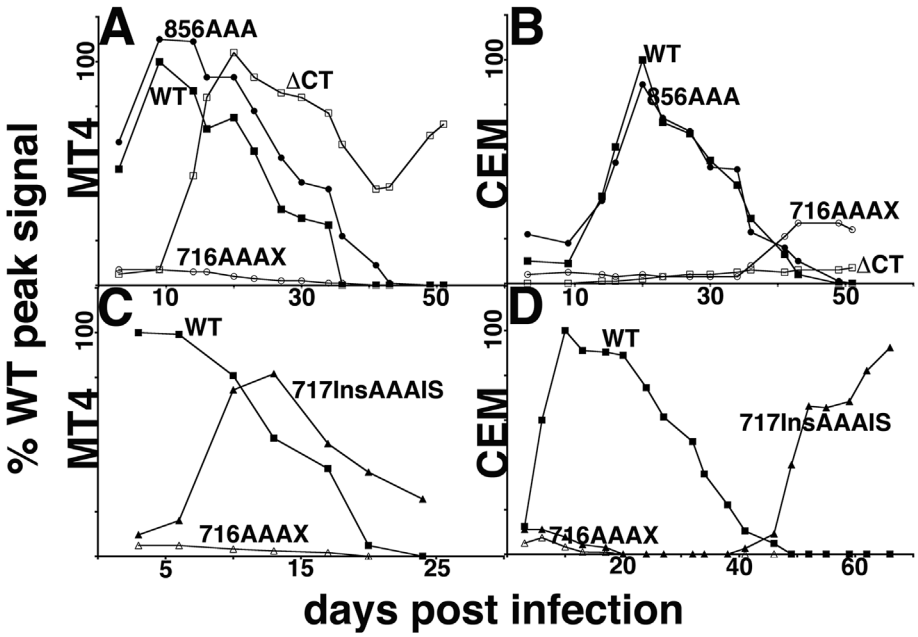

Fig. 3. Replication of WT, ΔCT, 716AAAX, 856AAA, and 716Ins variants in permissive and restrictive cells. For panels A–D, Gag-normalized stocks of WT (black squares), ΔCT (white squares), 856AAA (black circles), 716AAAX (white circles in A-B, white triangles in C-D), and 716AAAIS (black triangles) viruses produced in 293T cells were used to infect permissive MT-4 (MT4) or restrictive CEM-SS (CEM) T cells. Replication kinetics were tracked by monitoring cell-associated Gag levels at the indicated timepoints after infection, and Gag levels were normalized as percentages of the highest observed Gag level of the WT infection run in parallel (% WT peak signal). Note that viruses from the delayed (60 day) 716Ins replication peak in CEM-SS cells (panel D) were used subsequently to test for phenotypic reversion.

Fig. 4C-D, WT, ΔCT and parental 716Ins viruses replicated in MT-4 and CEM-SS cells as observed previously (Fig. 3A–D, Fig. 4A-B). Importantly, viruses from the cloned 716Ins-R* stock demonstrated similar replication kinetics as the original uncloned 716Ins-R stock, with rapid replication in MT-4 cells, and only slightly delayed replication (relative to WT virus) in CEM-SS cells. These results indicate that the sequence changes in 716Ins-R* were sufficient to confer a nearly WT HIV-1 replication phenotype.

2.2. Protein analysis of env truncation and small insertion variants

To assess how Env variants might alter Env protein localization patterns, we performed indirect immunofluorescence localization of Env proteins in cells transfected with a subset of the HIV-1 NL4-3 based constructs, using a primary antibody to the gp41 membrane-proximal external region (MPER; antibody 2F5) that is unaltered in all variants. Images of WT HIV-1 Env yielded a characteristic staining pattern with a single bright fluorescent spot adjacent to cell nuclei that we interpret to include RER, Golgi and/or multivesicular body (MVB) staining (Fig. 5, top panel). Relative to the WT pattern, we consistently observed an enhanced surface staining pattern for ΔCT Env (Fig. 5, top panel). Of the remaining variants, the 716Ins and 716Ins-R* Env proteins gave bright nuclear-adjacent spots, similar to WT Env; the 813X protein showed bright nuclear-adjacent spots as well as additional cellular staining; and the 716AAAX protein showed more diffuse nuclear-adjacent staining than WT (Fig. 5, top panel). In an effort to categorize staining patterns for each Env variant, we calculated the percentages of total cell Env staining that localized to single bright nuclear-adjacent spots from multiple cells (Fig. 5, bottom right). Consistent with the images in the top panel of Fig. 5, about 30% of WT Env localized to single nuclear-adjacent spots, while less than 15% of ΔCT Env did. The other variants gave intermediate values, with 716AAAX Env levels almost as low as those of ΔCT. However, in contrast with ΔCT Env, the 716AAAX Env proteins did not stain cell surfaces, but rather, showed a

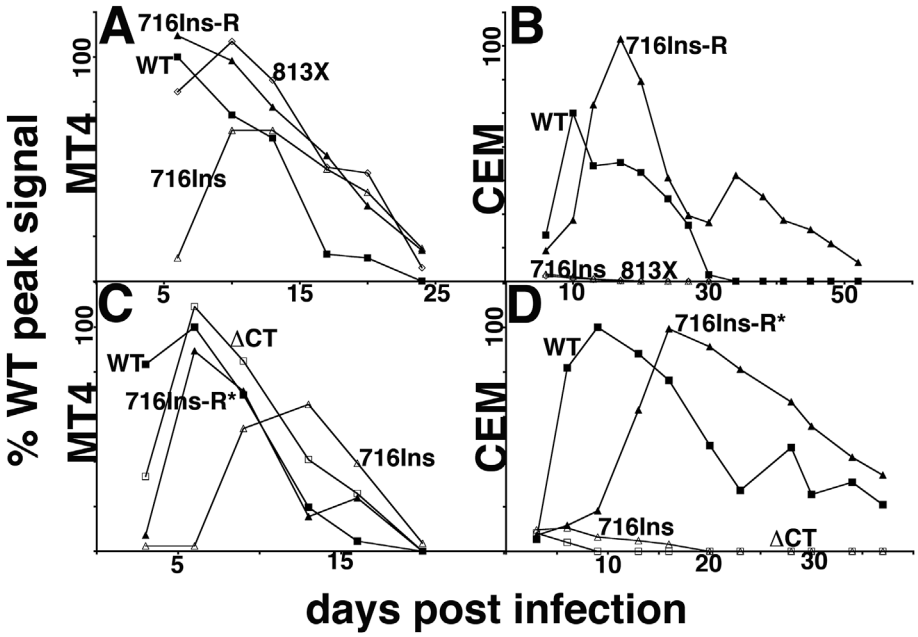

Fig. 4. Replication of WT, ΔCT, 813X, and 716Ins revertants in permissive and restrictive cells. Replication kinetics of WT (black squares), ΔCT (white squares), 813X (white diamonds), 716Ins (white triangles), 716Ins-R (black triangles in panels A-B), and 716Ins-R* (black triangles in panels C-D) viruses in permissive MT-4 (MT4) and restrictive CEM-SS (CEM) cells were monitored as described in the legend to Fig. 3. Note that the 716Ins-R virus stock derives from viruses collected from the late replication peak of the 716Ins infection of CEM-SS cells in Fig. 3D. The 716Ins-R* stock was generated by introducing the CT sequence changes identified in 716Ins-R (Fig. 1) into the 716Ins backbone.

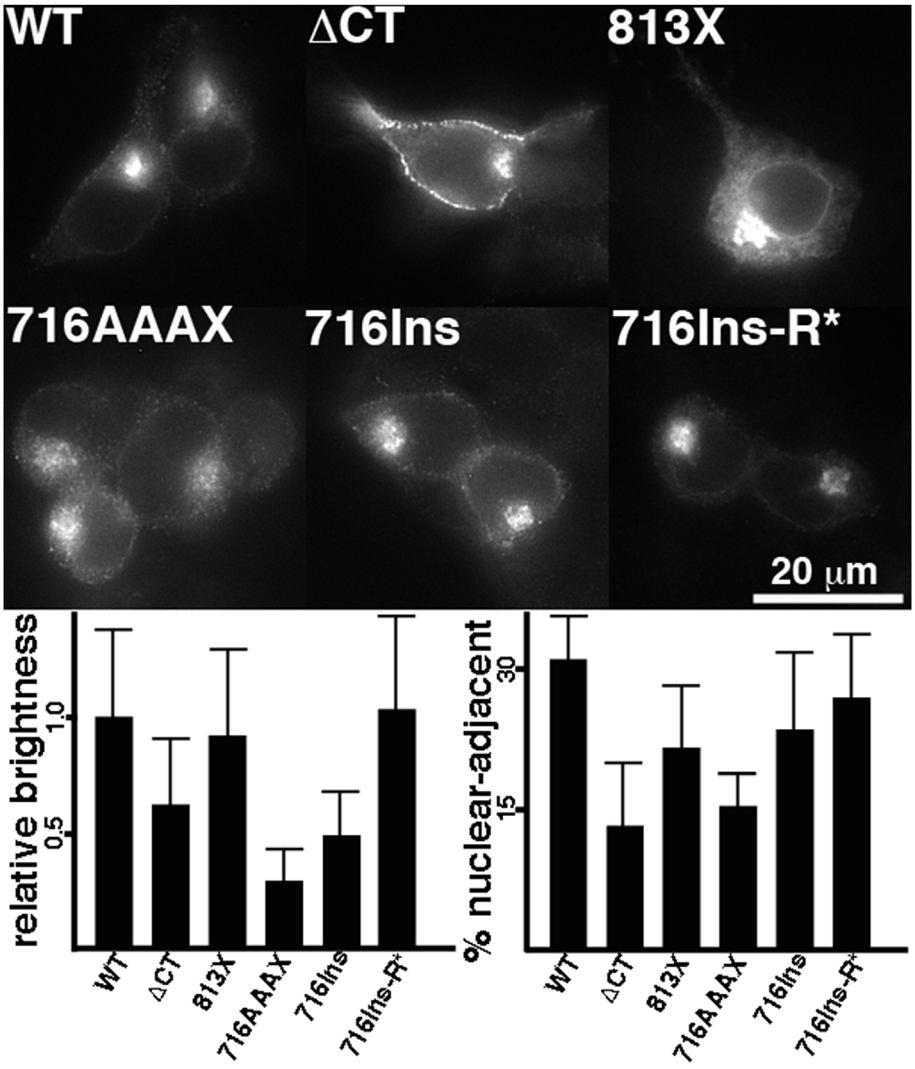

Fig. 5. Immunofluorescence analysis of CT truncation and insertion mutants. 293T cells were transfected with HIV-1 proviral constructs expressing the indicated CT variants, and Env proteins were detected via indirect immunofluorescence microscopy using a primary anti-gp41(MPER) antibody. The top panel shows examples immunofluorescence staining patterns of the indicated variants, where the size bar (20 μm) pertains to all images, and exposure times were chosen to achieve similar non-saturating brightness levels. The bottom left panel shows brightness levels of the indicated CT variants (relative to WT), determined as described in the Materials and Methods. Brightness averages derive from 47 (WT), 37 (716AAAX), 35 (ΔCT, 716Ins, 716Ins-R*) or 20 (813X) independent measurements. The bottom right panel shows the percentages of total cell brightness signals that localized to single nuclear-adjacent spots, as a rough indicator of nuclear-adjacent versus cytoplasmic or cell surface staining differences. Percentage nuclear-adjacent staining levels were determined as described in the Materials and Methods, and derive from 42 (813X), 34 (ΔCT), 33 (716Ins), 31 (716AAAX), 28 (716Ins-R*) or 23 (WT) independent measurements.

pattern of heterogeneous intracellular staining that we discuss below.

In addition to supplying rough comparisons of Env protein localization, our immunfluorescence data permitted us to compare Env expression levels via the monitoring of fluorescence brightness values from multiple cells (Fig. 5, bottom left). Our measurements showed that ΔCT, 813X, and 716Ins-R* Env expression levels all were at least 63% those of WT Env. However, by this metric, the 716Ins parental Env levels were less than half that of WT Env, and 716AAAX Env levels were 30% of WT Env values.

As an alternative approach for Env protein analysis, cell and virus protein samples from transfected cells were fractionated by electrophoresis, and immunoblotted for Gag and Env protein detection (Fig. 6). Our analyses of cell and viral Gag proteins showed characteristic precursor Gag (PrGag) and capsid (CA) staining patterns, with roughly similar cellular and viral levels for all of our HIV-1 NL4-3 Env protein variants (Fig. 6, left panels). These results imply that none of the Env variant constructs disrupted 3′ splice acceptor usage (see Fig. 1) that is required for Rev and Tat expression. Whereas Gag protein results appeared equivalent for the different variants, differences were observed for Env proteins (Fig. 6, right panels). Using an anti-gp41(MPER) primary antibody, WT and ΔCT proteins gave the expected results: WT gp160 and gp41 proteins were detected in cells and viruses, as were their lower molecular weight ΔCT counterparts. Consistent with immunofluorescence results, 716AAAX and 716Ins Env levels were significantly reduced relative to WT Env levels. In particular, cellular gp160 bands were demonstrably fainter than corresponding WT or ΔCT gp160 bands, and gp41 band intensities were barely above mock levels. Viral 716AAAX and 716Ins Env levels were even more reduced, relative to their counterparts. Results for the cloned 716Ins revertant (716Ins-R*; far right lanes) also were consistent with immunofluorescence results. Specifically, cell and viral gp160 and gp41 bands were roughly as bright as WT and ΔCT controls. However, two distinct gp41 bands were apparent, especially in the 716Ins-R* viral sample. These bands migrated approximately at the sizes of the WT and ΔCT gp41 proteins, suggesting that 716Ins-R* Env is processed both at the appropriate gp120/gp41 cleavage site, but also at a site closer to membrane. Similar, fainter bands also were observed in virus samples of the 716Ins parent, and these observations are discussed below.

We quantified Env levels from cell and viral samples in multiple experiments on cells transfected with the NL4-3, ΔCT, 813X, 716AAAX, 716Ins, 716Ins-R* and 856AAA proviral constructs (Fig. 7). As shown, all but two of the variants expressed approximately WT levels of Env in cells, and contained Env levels approximately equal to or higher than WT Env levels in virus particles. The two exceptions were 716AAAX and 716Ins, which respectively yielded cellular Env levels of one quarter and one third that of WT Env, and viral Env levels of less than 10% WT levels. Despite this, it is worthwhile to note that 716Ins viral Env levels were sufficient to support viral replication, at least in the context of MT-4 cells (Figs. 3C, 4A, 4C).

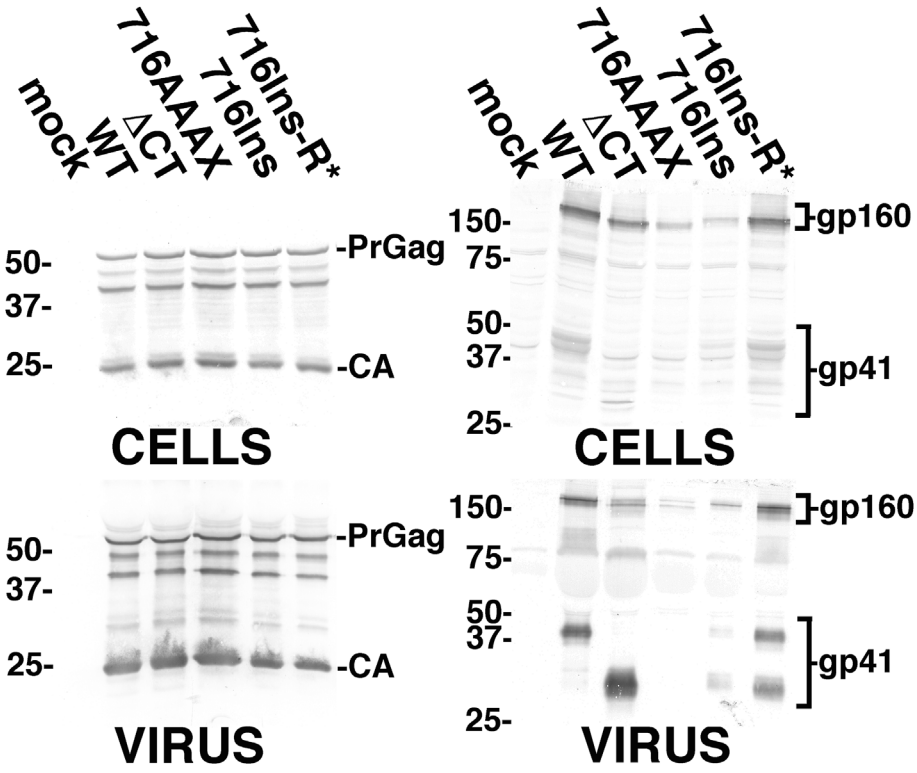

Fig. 6. Gag and Env compositions in cells and viruses. Cell lysate and virus samples were prepared from 293T cells transfected with the indicated HIV-1 proviral expression constructs, fractionated by electrophoresis, and subjected to immunoblot detection of Gag and Env proteins using primary anti-CA or anti-gp41(MPER) antibodies. The migration positions of PrGag, CA, gp160 and gp41 positions are as indicated, as are the positions of 150, 75, 50, 37, and 25 kDa molecular weight markers run in parallel. Viral CA to PrGag ratios were as follows: WT, 1.7; ΔCT, 1.9; 716AAAX, 1.6; 716Ins, 1.7; 716Ins-R*, 1.5. Viral total gp41 to gp160 ratios were as follows: WT, 1.3; ΔCT, 6.0; 716AAAX, 0.01; 716Ins, 0.8; 716Ins-R*, 1.3. For 716Ins variants, ratios of cleaved to uncleaved gp41 were: 716Ins, 3.0; 716Ins-R*, 1.0.

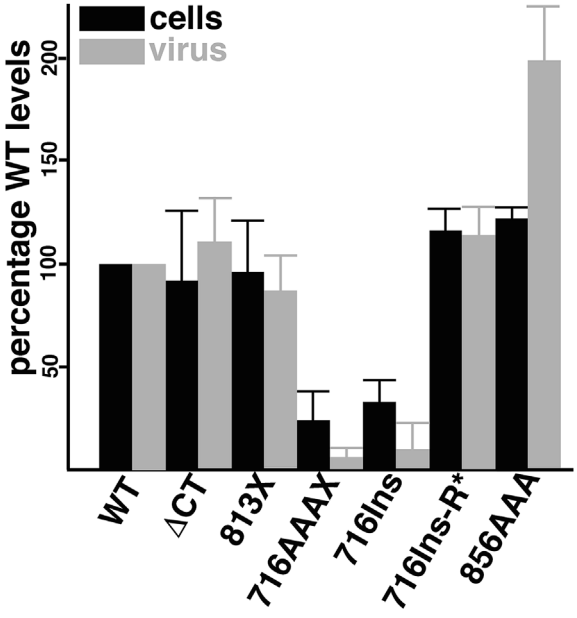

Fig. 7. Envelope protein levels in cells and viruses. Cell and virus Env protein levels from transfected 293T cells were determined by densitometric quantitation of Env signals from immunoblots as exemplified in Fig. 6. Levels were normalized as percentages of WT Env levels from experiments performed in parallel. Measurements derive from 7 (WT), 5 (813X), 4 (716Ins, 716Ins-R*), 3 (ΔCT, 716AAAX), or 2 (856AAA) independent measurements.

2.3. Analysis of viruses with C-terminal env protein tags

Given that the 856AAA virus replicated with WT virus kinetics in both MT-4 and CEM-SS cells (Fig. 3A-B), we decided to examine HIV-1 NL4-3-based viruses with Env CT C-terminal Flag epitope, green fluorescence protein (GFP), vesicular stomatitus virus G protein cytoplasmic tail (Gtag), and promiscuous biotin ligase (BirA*) tags (Brizzard and Chubet, 2001; Zhang et al., 1996; Turner et al., 1996; Roux et al., 2012; Ritchie et al., 2015, Fig. 1). Thus, viruses generated in 293T cells were used to infect MT-4 and CEM-SS cells, and replication was tracked as described for Figs. 3-4. Once again, WT viruses replicated well in both cell types, while ΔCT viruses replicated with slightly delayed kinetics in MT-4 cells, but were defective in CEM-SS cells (Fig. 8). Interestingly, the viruses with Env proteins carrying the four C-terminal tags showed different replication profiles. The Flag virus replicated well in both MT-4 and CEM-SS cells; the GFP virus replicated well in MT-4 cells, but poorly in CEM-SS cells; the Gtag virus showed an early replication peak in MT-4 cells, and a late replication peak in CEM-SS cells; and the BirA* virus did not replicate in CEM-SS cells, and showed a late replication peak in MT-4 cells (Fig. 8). Notably, viruses collected from the BirA*-MT-4 late replication peak proved to be revertants that had completely deleted the BirA* sequence (data not shown).

Because of their potential practical use, we chose to examine the Flag and GFP viruses in more detail. To do so, we collected WT and Flag viruses from Fig. 8C day 3 infections and GFP viruses from Fig. 8C day 10 viruses. These viral stocks then were employed in infections of new MT-4 or $CD4^+$ HeLa (HiJ; Kabat et al., 1994) cells. At three days post-infection, cells were processed for dual fluorescence analysis with a primary 2F5 anti-gp41(MPER) antibody, and either GFP, a primary antibody to GFP, or an anti-Flag primary antibody. Significantly, we found that intrinsic GFP fluorescence from the GFP-tagged Env protein did not yield a robust, reliable signal, either from the aforementioned GFP virus stock, or from GFP virus stocks produced freshly by transfection of 293T cells (data not shown): these results suggest that the specific positioning of the EGFP coding region in our C-terminally Env-tagged construct was suboptimal for GFP fluorescence in infected cells. However, as shown in Fig. 9, both Flag and GFP tags were readily detected via indirect immunofluorescence protocols using primary anti-Flag and anti-GFP antibodies. In particular, for both infected MT-4 and HiJ cells, Flag or GFP signals largely co-localized with gp41(MPER) signals, with predominant nuclear-adjacent staining patterns similar to those observed in Fig. 5. Calculation of Pearson's correlation coefficients for colocalization were 0.91 ± 0.05 for the Flag virus in MT-

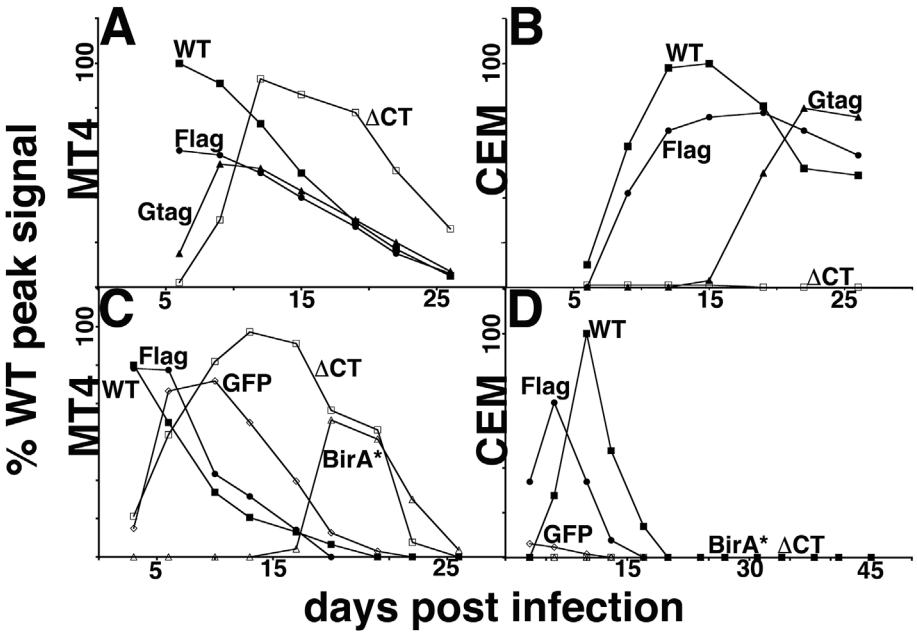

Fig. 8. Replication of WT, ΔCT, Flag, Gtag, GFP, and BirA* viruses in permissive and restrictive cells. Replication kinetics of WT (black squares), ΔCT (white squares), Flag (black circles), Gtag (black triangles), GFP (white diamonds), and BirA* (white triangles) viruses in permissive MT-4 (MT4) and restrictive CEM-SS (CEM) cells were monitored as described in the legend to Fig. 3. Viruses were as described in Fig. 1. Note that viruses from the delayed (20 day) BirA* replication peak in MT-4 cells (panel C) were used subsequently to test for phenotypic reversion, and were found to have deleted the BirA* coding region. Panel C WT and Flag virus samples collected at day 3, and GFP viruses collected at day 10 were used to infect new target cells for immunofluorescence analysis as shown in Fig. 9.

4 cells, 0.92 ± 0.03 for the Flag virus in HiJ cells, 0.85 ± 0.08 for the GFP virus in MT-4 cells, and 0.79 ± 0.05 for the GFP virus in HiJ cells. These results indicate that Flag or GFP tags are retained in the same compartments as gp160 or gp41 proteins, at least at the resolution of conventional fluorescence light microscopy (~270 nm; Davidson, 2019).

We further examined Flag and GFP viruses in parallel with WT HIV-1 via immunoblot analysis of viruses produced by transfection of 293T cells that had been mock-treated or treated with the HIV-1 protease (PR) inhibitor, ritonavir (Fig. 10). As expected, Gag levels for the WT, Flag, and GFP viruses were similar, and were skewed to show more precursor GagPol (PrGP) and precursor Gag (PrGag) proteins in ritonavir-treated samples (Fig. 10, left panel). Probing the viral proteins with the anti-gp41(MPER) antibody (Fig. 10, center panel) revealed WT gp160 and gp41 bands in both treated and untreated cells. As expected, GFP viruses showed higher molecular weight gp160 and gp41 bands, reflective of the addition of the 27 kDa (Zhang et al., 1996) GFP tag. However, we also observed GFP virus gp41 bands of approximately WT size that were more prominent in untreated versus ritonavir-treated cells: these results suggest that some of the GFP virus gp41-GFP fusion protein is processed to yield a gp41-sized moeity, and that HIV-1 PR is responsible for at least some of this processing.

We also obtained evidence that the gp41-Flag and gp160-Flag proteins produced by the Flag virus were subjected to processing by cellular protease action in 293T cells. Notably, using the anti-gp41(MPER) antibody, instead of a gp41-Flag-sized band, a faster migrating band of ~25–30 kDa was observed for the mock-treated sample (Fig. 10, middle panel, second lane from left). A slightly lower mobility band was observed for the Flag virus in the ritonavir-treated sample (Fig. 10, middle panel, second lane from right), suggesting a combination of viral and cellular protease action in the CT of the Flag Env protein. Further evidence for Flag Env processing was provided by probing viral proteins with the Chessie 8 (anti-gp41[CT]) antibody, which has an epitope corresponding to Env residues 727–732 (Abacioglu et al., 1994, Fig. 1). Here (Fig. 10, right panel), while WT and GFP viruses exhibited gp160 and gp41 bands similar to those observed with the anti-gp41(MPER) antibody, nothing was observed for the Flag virus produced either in the presence or absence of ritonavir. These results imply that Flag Env proteins either are cleaved at the Chessie 8 epitope, or on the membrane side of the epitope such that the predicted ~20 kDa CT-Flag product was not observed. Interestingly, when we probed Flag viruses isolated from peak fractions of CEM-SS infections (Fig. 8B, infection

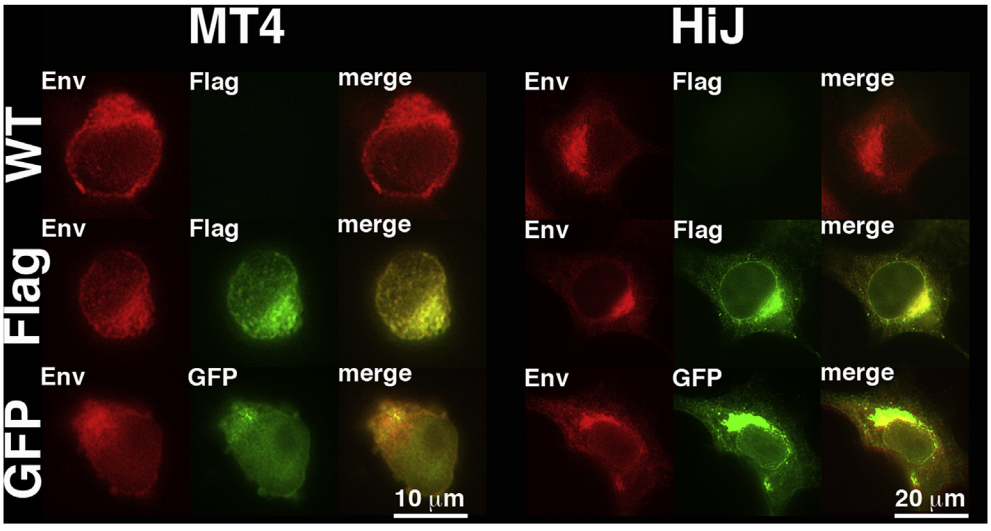

Fig. 9. Immunofluorescence analysis of cells infected with WT, Flag, and GFP viruses. Viruses were collected from day 3 (WT, Flag) or day 10 (GFP) of the MT-4 infections shown in Fig. 8, panel C and used to infect new MT4 or HiJ ($CD4^+$ HeLa) cells. Three days post-infection, cells were processed for immunofluorescence analysis using the indicated anti-Env (gp41 MPER), Flag and GFP antibodies. Size bars for all MT4 images (10 μm) and all HiJ images (20 μm) are as shown. Pearson's correlation coefficients for colocalization were as follows: Flag virus, MT4 cells: 0.91 ± 0.05 (n = 15); Flag virus HiJ cells 0.92 ± 0.03 (n = 19); GFP virus, MT4 cells: 0.85 ± 0.08 (n = 10); GFP virus, HiJ cells 0.79 ± 0.05 (n = 8).

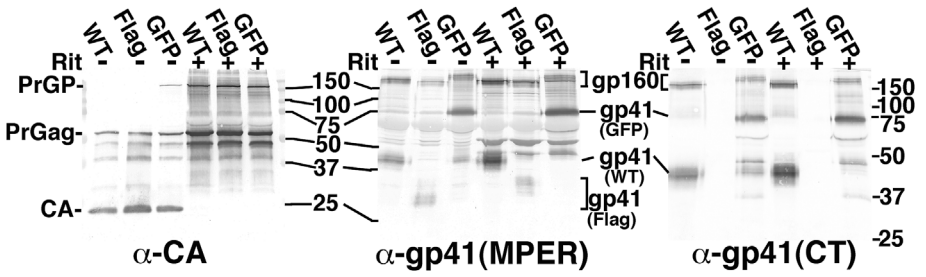

Fig. 10. Analysis of WT, Flag, and GFP viruses. HIV-1 viruses were collected from mock-treated (Rit -) or ritonavir-treated (Rit +) 293T cells transfected with WT, Flag or GFP proviral expression constructs (Fig. 1). Aliquots of viral samples were fractionated by electrophoresis and immunoblotted using the indicated primary antibodies. Migration positions of 150, 100, 75, 50, 37 and 25 kDa marker proteins run in parallel lanes are as shown, as are the positions of PrGag-Pol (PrGP), PrGag, CA, gp160, and the specific gp41 proteins [gp41(WT), gp41(Flag), gp41(GFP). Note that Flag viruses were not detected with the α-gp41(CT) antibody, indicative of a CT processing event. In the α-CA panel, CAto PrGag ratios were as follows: WT-, 1.4; Flag-, 2.5; GFP-, 1.8; all ritonavir + samples, 0.0. In the MPER panel, specific gp41 to gp160 ratios were as follows: WT-, 1.0; Flag-, 1.0; GFP-, 1.9; WT+, 1.4; Flag+, 0.3; GFP+, 1.7. In the CT panel, specific gp41 to gp160 ratios were as follows: WT-, 1.6; GFP-, 2.7; WT+, 1.8; GFP+, 2.1. Note that ratios of processed (~41 kDa) versus unprocessed (~70 kDa) gp41(GFP) species were as follows: GFP-(α-MPER), 0.3; GFP+(α-MPER), 0.0; GFP-(α-CT), 0.7; GFP+(α-CT), 0.1.

days 7–17), we observed full-length gp41-Flag proteins, in addition to C-terminal ~24 kDa CT-Flag fragments (data not shown). These results indicate that the efficiency of processing C-terminally Flag-tagged Env proteins was cell-type dependent.

3. Discussion

Our investigations on the replication of HIV-1 Env variant viruses have led to a number of novel observations. With WT and ΔCT Env control viruses, we have confirmed the inability the ΔCT variant to replicate in restrictive cells (Murakami and Freed, 2000a; Qi et al., 2013, 2015; Kirschman et al., 2018), and frequently have observed slight ΔCT delays in permissive MT-4 cells (Figs. 3A, 8A, 8C). In addition to the previously described (Freed and Martin, 1995) ΔCT truncation mutant, we also characterized 716AAAX and 813X truncations. The 716AAAX viruses were dead in both permissive and restrictive cells (Fig. 3), and 716AAAX Env protein levels were dramatically reduced in both transfected cells and viruses produced by transfected cells (Figs. 5–7). A notable difference between 716AAAX and ΔCT Env proteins is that the former retains the YxxL AP-2 recognition motif (Checkley et al., 2011; Qi et al., 2013, 2015; Kirschman et al., 2018; Ohno et al., 1997; Boge et al., 1998, Fig. 1). Given this, our interpretation for observing low 716AAAX Env protein levels is that the proteins traffic to cell surfaces, are internalized via clathrin-mediated endocytosis and, lacking signals to be recycled to cell surfaces, they are shunted off for lysosomal degradation. Our results with the 813X viral variant are more intriguing. When produced in 293T cells, a similar truncation mutant Env protein was incorporated into virions, and retained fusion activity (Jiang and Aiken, 2007). Our current investigations showed that this variant had a phenotype similar to that of ΔCT (Fig. 4A-B), replicating well in MT-4 cells but replication-defective in CEM-SS cells. However, the 813X virus encodes both the AP-2 binding site and YW residues implicated in FIP1C binding (Qi et al., 2013, 2015) that are present in WT HIV-1 NL4-3 genomes. This suggests that interactions of Env CT C-terminal residues with viral and/or cellular factors are necessary for Env protein incorporation into or function within viruses produced in restrictive cell lines.

Given that the N-terminal portion of the HIV-1 CT appears to be unstructured (Murphy et al., 2017), we did not expect the small insertion after the AP-2 binding site in the 716Ins virus (Fig. 1) to affect virus function. Nevertheless, like the ΔCT virus, the 716Ins virus replicated in MT-4 cells, but not in CEM-SS cells (Figs. 3-4). Significantly, the mutations present in the cloned 716Ins revertant, 716Ins-R*, were sufficient to confer replication capacity in CEM-SS cells, but the mechanism for this phenotypic change is unclear. The most significant difference observed in transfected cells for the 716Ins variant versus WT or 716Ins-R* was the reduction in Env protein levels (Figs. 5–7). Thus, a simple hypothesis is that 716Ins Env expression levels are not adequate enough to guarantee HIV-1 replication in CEM-SS cells, but suffice for MT-4 cells. However, one potential complication for interpretation of 716Ins or 716Ins-R* replication was the occurrence of gp41-related bands of the same size as ΔCT gp41 (Fig. 6, far right lanes). This cleavage pattern is reminiscent of that observed previously for the CT P714L and S716L mutations that confer resistance to the cholesterol binding compound, amphotericin B methyl ester (Waheed et al., 2006, 2007), suggesting that the membrane proximal portion of the HIV-1 CT is particularly sensitive to proteolytic processing.

As shown in Fig. 8, with C-terminally tagged HIV-1 Env proteins, variable results were observed. In the extreme case, BirA* viruses appeared dead, and deletion of the BirA* coding region was selected in the process of phenotypic reversion. Gtag and GFP viruses represented intermediate cases: they replicated efficiently in MT-4 cells, and either not at all (GFP), or with significantly delayed kinetics (Gtag) in CEM-SS cells (Fig. 8). In contrast, the Flag (Fig. 8) and 856AAA (Fig. 3) viruses both replicated efficiently in both cell lines tested. To ensure that Flag and GFP sequences were not lost during replication, virus stocks were collected at MT-4 infection peaks and used to infect new cells. As shown in Fig. 9, the Flag and GFP coding regions were retained in the Flag and GFP viruses, and Flag and GFP tags colocalized with Env in infected cells. However, there are two notable caveats. Firstly, while we observed a strong GFP signal using an indirect immunofluorescence approach with an anti-GFP antibody, we did not observe reproducible intrinsic GFP signals: we conjecture that the specific environment of GFP in our gp41-GFP proteins was not optimal for GFP fluorescence. The second caveat is that we observed cell type-dependent processing of gp41-Flag proteins.

Viruses produced by 293T cells showed truncated gp41 proteins with the anti-gp41(MPER) antibody, and the absence of detectable Env proteins using the Chessie 8 anti-gp41(CT) antibody (Fig. 10). However, in addition to truncated CT-Flag proteins, full-length gp41-Flag proteins were observed in viruses from infected CEM-SS cells (data not shown). These results are indicative of cell type-dependent Env processing events, underscore the flexibility of HIV-1 in overcoming potentially deleterious Env changes or environmental conditions (Waheed et al., 2006, 2007; Checkley et al., 2011), and indicate there is still much to learn about the mechanisms by which HIV-1 Env proteins operate.

4. Materials and methods

Cells. Human HeLa (Scherer et al., 1953) cells were obtained from the American Type Culture Collection (ATCC) and grown in humidified 5% carbon dioxide air at 37 °C in Dulbecco's Modified Eagle's Media (DMEM) supplemented with 10% fetal bovine sera (FBS) plus 10 mM Hepes pH 7.3, penicillin and streptomycin. HEK293T (293T) cells (DuBridge et al., 1987) were obtained from the laboratory of David Johnson (OHSU) and were grown similarly to HeLa cells. HiJ cells are a $CD4^+$ variant of HeLa cells (Kabat et al., 1994) that were obtained from the laboratory of Dr. David Kabat (OHSU) and also were grown similarly to HeLa cells. MT-4 and CEM-SS T cell lines were obtained from the NIH Aids Reagent Program and were grown in Roswell Park

Memorial Institute (RPMI) media plus 10% FBS, Hepes, penicillin and streptomycin.

Viral constructs. The proviral molecular clones to WT and ΔCT (CT144; Freed and Martin, 1995) HIV-1 strain NL4-3 (Adachi et al., 1986) were obtained from Dr. Eric Freed (NCI Frederick). The 813X variant was produced by inserting a palindromic oligonucleotide into the NL4-3 nucleotide (nt) 8648 HpaI site to yield the sequence gct gtt **aac** tag cgc tag tta ac, where the bold font codon encodes Env residue 813, and the underlined codons are termination codons. The 716AAAX and 856AAA constructs were generated by polymerase chain reaction (PCR) directed mutagenesis to create NotI restriction enzyme sites (encoding AAA) and termination codons after Env residues 716 and 856. For 716AAAX, the NL4-3 8351–8368 sequence was replaced with tca cca tta **tcg** *gcg gcc gcg* taa tca cca tta tcg ttt cag, where the bold font codon encodes residue 716, the three alanine codons are italicized, the termination codon is underlined, and the final codon is the one before the third Rev exon 3′ splice site. For 856AAA, the NL4-3 8777–8792 sequence was replaced with ttg **cta** *gcg gcc gcg* tga ttt tgc tat aag ATG ggt, where the bold font codon encodes residue 856, the three alanine codons are italicized, the termination codon is underlined, and the upper case codon is the first codon of the *nef* gene. The 716Ins variant was constructed from 716AAAX by insertion of a PCR-amplified NL4-3 fragment to replace the NL4-3 8351–8368 sequence with tca cca tta **tcg** *gcg gcc gcg ata tcg* ttt cag, where the bold font codon encodes residue 716, the italicized codons encode the five residue AAAIS insert, and the final codon is the one before the third Rev exon 3′ splice site. The 716Ins-R* variant was made by replacing the 716AAAX NotI-XhoI (NL4-3 nt 8887) fragment with the homologous PCR-amplified fragment from the cloned 716Ins revertant. The sequence of 716Ins-R* is identical to that of 716Ins except for codon 717 (ttt to ctt, encoding F to L) and codon 737 (ggt to gat, encoding G to D). The Flag, GFP, Gtag, and BirA* variants all were generated from 856AAA by insertion of versions of the tags that carried NotI sites at 5′ and 3′ ends. The Flag insert encodes three repeats of the Flag epitope (Brizzard and Chubet, 2001) with the following sequence: gcg gcc gcc ctc gag gga ggc ggt gga gcc gac tac aag gac cac gac ggc gac tac aag gac cac gac atc gac tac aag gac gac gac gac aag ggg ccc gtt taa acc cgc tga tcc gcg gcc gcg, where the termination codon is underlined. The GFP variant encodes EGFP (Zhang et al., 1996), with a 5′ juncture sequence of 5′ gcg gccgca ccg gtc gcc acc ATG gtg agc aag ggc 3′, where the upper case codon is the EGFP initiation codon; and a 3′ juncture sequence of 5′ ctg tac aag tac **tca** gat ctg gcg gcc gcg tga 3′, where the codon in bold is the last codon of GFP, and the termination codon is underlined. The Gtag variant encodes the VSV G protein cytoplasmic tail (Turner et al., 1996) at the C-terminus of 856AAA, with the sequence gcg gcc gca cga gtt ggt atc cat ctt tgc att aaa tta aag cac acc aag aaa aga cag att tat aca gac ata gag atg aac cga ctt gga aag taa gct tgc ggc cgc, where the termination codon is underlined. The BirA* variant encodes the promiscuous bacterial biotin ligase (BirA*; Roux et al., 2012; Ritchie et al., 2015) , with a 5′ juncture sequence of 5′ gcg gcc gca aag ctt cat ATG 3′, where the upper case codon is the initiation codon of Myc-tagged BirA* (Roux et al., 2012; Ritchie et al., 2015), and a 3′ juncture sequence of 5′ ctc gag gcg gcc gcg tga 3′, where the termination codon is underlined.

Virus propagation and sample processing. For analysis of NL4-3-based viruses, confluent 10 cm plates of 293T cells were transfected with 24 μg DNA, using calcium phosphate or polyethyleneimine (PEI) methods (Barklis et al., 2018). For immunofluorescent localization of viral proteins in transfected cells, cells were split one day post-transfection 1:20 and 1:40 onto 22 × 22 mm polylysine-treated coverslips in six well plates. For this protocol, coverslips were pre-rinsed in ethanol, flamed, incubated 5 min at room temperature in 0.1 mg/ml polylysine (Sigma P4707), rinsed 2 min with phosphate-buffered saline (PBS; 9.5 mM sodium potassium phosphate [pH 7.4], 137 mM NaCl, 2.7 mM KCl), supplemented with growth media, seeded with transfected cells, grown 2 d, and processed for immunofluorescence as described below. For analysis of viral proteins, virus and cell samples were collected from transfected 10 cm plates of cells at 3 d post-transfection. To do so, virus-containing media samples (10 ml) were filtered through 0.45 μm filters (Millipore), concentrated by centrifugation through 2 ml 20% sucrose in PBS cushions (1 h at 197,000 x g; 40,000 rpm, Beckman SW41 rotor), suspended in 0.1 ml PBS, mixed with 0.1 ml of 2 x sample buffer (12.5 mM Tris-HCl [pH 6.8], 2% sodium dodecyl sulfate [SDS], 20% glycerol, 0.25% bromphenol blue) plus 0.1 volume of β-mercaptoethanol (BME), and stored frozen prior to analysis as described below. Cell samples for protein analysis were prepared by collecting cells in PBS, pelleting 20% of the cell sample, suspension in 50 μl IPB (20 mM Tris-HCl [pH 7.5], 150 mM NaCl, 1 mM ethylenediamine tetraacetic acid [EDTA], 0.1% SDS, 0.5% sodium deoxycholate, 1.0% TritonX-100, 0.02% sodium azide), vortexing, incubation on ice for 5 min, pelleting 15 min at 13,000 x g to remove insoluble debris, mixing with 50 μl 2 x sample buffer plus 0.1 vol BME, and stored frozen prior to analysis.

In experiments where viruses were used to infect MT-4 or CEM-SS cells, at three days post-transfection, virus-containing media supernatants were filtered through 0.45 μm filters and stored at −80 °C while aliquots were monitored for Gag protein levels. To do so, unpelleted virus-containing media samples (50 μl) were mixed with 50 μl 2 x sample buffer plus 5 μl BME and processed for Gag protein quantitation as described below. For longitudinal infections, Gag-normalized virus amounts were inoculated into flasks of MT-4 or CEM-SS cells. After infections were initiated, aliquots of cells (20%) were collected every 3–4 d, pelleted, suspended in 50 μl IPB, mixed with 50 μl 2 x sample buffer plus 5 μl BME, and processed for Gag protein quantitation. Replication kinetics were plotted by quantitation of Gag levels in samples at all collection dates, and normalization to the peak date Gag value of a WT NL4-3 infection performed in parallel. In some cases, potential revertant viruses from late stage collections were used to re-infect fresh stocks of cells after normalization of Gag levels with control virus stocks to be employed in parallel infections. These passages were monitored by immunoblotting as described above, and potential mutations were cloned as described below. We also used viruses collected at peak infection dates for infection of new MT-4 and HiJ cells, with the objective of performing immunofluorescence analysis of newly infected cells. For HiJ samples, cells that were seeded on polylysine-coated coverslips were infected, and processed for immunofluorescence at 3 d post-infection. For MT-4 samples, non-adherent cells were infected with virus samples for 3 d in solution, after which cells were pelleted, suspended in 50 μl paraformaldehyde (Sigma) in PBS, applied to polylysine-coated coverslips for 10 min, gently rinsed with PBS, and processed for immunofluorescence.

Immunofluorescence. Cells on coverslips prepared as described above were fixed 30 min in 4% paraformaldehyde in PBS at room temperature, washed in PBS, permeabilized in 0.2% Triton X-100 in PBS at room temperature for 10 min, washed once with PBS, and incubated 10 min in culture media. Subsequently, coverslips were incubated 1 h at 37 °C in media containing primary antibody, rocking every 15 min. After primary antibody incubations, coverslips were washed three times in culture media, and then incubated in media containing secondary antibody at 37 °C for 30 min, rocking once at 15 min. Following incubations, the cells were washed twice in culture media and three times in PBS, followed by mounting on microscope slides in Fluoro-G mounting medium. Primary antibodies employed in immunofluorescence studies were the following: mouse anti-HIV-CA hybridoma media (Hy183, kindly provided by Dr. Bruce Chesebro) at 1:15; mouse anti-gp41(CT) hybridoma media (Chessie 8 recognizing CT residues 727–732 [PDRPEG], from the NIH AIDS Reagent Program) at 1:15; human anti-gp41(MPER) (2F5, Polymun Scientific, Product AB001, Lot T580703-A, recognizing HIV-1 Env residues ELDKWA; kindly provided by Dr. Hermann Katinger) at 1:15,000; mouse anti-Flag M2 (Sigma F1804) at 1:5,000; and rabbit anti-GFP (Life Technologies, Thermo Fisher #A11122) at 1:3,000. Secondary antibodies employed in immunofluorescence studies were Alexa Fluor 488 or 594 conjugated goat anti-mouse, anti-rabbit, or anti-human antibodies (Invitrogen;

Thermo Fisher) used at 1:1000.

Samples were viewed on a Zeiss AxioObserver fluorescence microscope using 63x (Planapochromat; NA = 1.4) objective and a Zeiss filter set 10 (excitation bandpass 450–490; beamsplitter Fourier transform 510; emission bandpass 515–565) for green fluorophores, or Zeiss filter set 20 (excitation bandpass 546/12, beamsplitter Fourier transform 560, emission bandpass 575–640) for red fluorophores. Images were collected with Zeiss Axiovision software with a fixed gain setting of 100 and exposure times taken to maximize brightness levels without pixel saturation. Relative brightness levels were calculated by averaging exposure times of images collected for different samples. The reciprocals of these averaged exposure times were normalized to the average obtained for WT samples. For the purpose of presenting color images, gray-scale 16 bit TIFF images were converted to green or red images using the Image J (Schneider et al., 2012) Image/Lookup Tables function, and then saved as 8 bit RGB images. For overlays of red and green images, RGB TIFF images were opened in Adobe Photoshop, layered using the screen option, and flattened. Colocalization analysis of Env and Flag or GFP signals was performed by determining Pearson's Correlation Coefficient (PCC) values, which vary from −1 (inversely correlated) to +1 (completely correlated) (Adler and Parmryd, 2010). To do so, matched images in Image J were stacked, single cell areas without background regions were boxed and cropped, destacked, and then used as input for the Image J JACoP PCC Plugin (Schneider et al., 2012). To measure total brightness signals in cells that localized to single perinuclear spots, individual cells and their single most prominent perinuclear spots were outlined, and corresponding areas and average brightnesses were measured in Image J. Total cell and perinuclear spot brightness levels were calculated by multiplication of areas and average brightness levels, and percentages of perinuclear staining were determined by averaging of total perinuclear brightness levels versus total cell brightness levels.

Viral protein analysis. Cell lysate and virus samples for protein analysis were prepared as described above and subjected to SDS-polyacrylamide gel electrophoresis (SDS-PAGE) as described previously (Wang et al., 1993; Alfadhli et al., 2016; Ritchie et al., 2015; Barklis et al., 2018), except that samples for Env protein detection were not heated before electrophoresis, and acrylamide concentrations were either 10% or 7.5%. Typically, 15% viral samples or 6% cell samples were subjected to electrophoresis in parallel with molecular weight size standards (Bio-Rad). After SDS-PAGE fractionation, proteins were electroblotted and immunoblotted following previously described methods (Wang et al., 1993; Alfadhli et al., 2016; Ritchie et al., 2015; Barklis et al., 2018). Primary antibodies (see above) employed were as follows: Hy183 at 1:15, Chessie 8 at 1:15, 2F5 at 1:3,000; anti-Flag M2 at 1:5,000; anti-GFP at 1:3,000; anti-FIP1C (D9D8P; Cell Signaling Technologies #12849S) at 1:3,000; anti-β-actin (Thermo Fisher MA5-15739) at 1:3,000. Secondary antibodies (Promega) were antimouse, antirabbit, or antihuman IgG alkaline phosphatase-conjugated antobodies used at 1:15,000. Color reactions for visualization of antibody-bound bands employed nitrobluetetrazolium plus 5-bromo-4-chloro-3-indolyl phosphate in AP buffer (100 mM Tris-hydrochloride [pH 9.5], 100 mM NaCl, 5 mM MgCl2). For quantitation, immunoblots were air-dried and scanned using an Epson Perfection V600 scanner. Band intensities of scanned TIFF images were determined using NIH Image J software.

Revertant cloning. NL4-3 revertants cloned from longitudinal passages were isolated by extraction of DNA from infected cells. Cells were lysed in 250 µl IPB. An equal volume of water was added, and cells were then digested with 50 µg of proteinase K for 2 h. DNA was isolated by phenol-chloroform extraction and ethanol precipitation. Matrix and envelope regions of HIV-1 proviral DNAs were amplified using PfuUltra High Fidelity polymerase (Agilent) and NL4-3-based primers of nt 671–691 and 1219-1200 for MA, and 7449–7468 and 8892-8871 for Env. PCR products were A-tailed using Taq polymerase and 2 mM dATP, and then cloned into pGEMTeasy plasmids (Promega) for sequence analysis. For BirA* and 716Ins revertant sequencing, no MA changes were observed, the BirA* coding region was deleted, and point mutations were observed at Env CT codons 717 and 737 for the 716Ins revertant (716Ins-R), as indicated in Fig. 1. To generate a molecular clone (716Ins-R*) that was identical to 716Ins except for the two 716Ins-R mutations, the sequenced revertant pGEMTeasy NotI (at CT residue 716) to XhoI (NL4-3 nt 8887) NL4-3-derived sequence was used to replace the homologous sequence from 716AAAX.

Conflicts of interest

The authors declare no conflict of interest.

Declarations of interest

None.

Acknowledgements

We thank Drs. David Kabat and Bruce Chesebro respectively for supplying the HiJ and Hy183 cell lines. The Chessie 8, CEM-SS and MT-4 cell lines were obtained from NIH Aids Reagent Program, and the anti-gp41(MPER) 2F5 antibody was kindly supplied by Dr. Hermann Katinger (Polymun Scientific). We are grateful for help, advice, and assistance from Logan Harper, Andrew Mack, Roland Max Petty, Christopher Ritchie, and Fikadu Tafesse. This research was supported by NIH grant R01 GM060170.

References

Davidson, M.W., 2019. Numerical aperture and image resolution. https://.www.microscopyu.com/.tutorials/.imageformation-airyna.

Abacioglu, Y., Fouts, T., Laman, J., Claassen, E., Pincus, S., Moore, J., Roby, C., Kamin-Lewis, R., Lewis, G., 1994. Epitope mapping and topology of baculovirus-expressed HIV-1 gp160 determined with a panel of murine monoclonal antibodies. AIDS Res. Hum. Retrovir. 10, 371–381.

Adachi, A., Gendelman, H., Koenig, S., Folks, T., Willey, R., Rabson, A., Martin, M., 1986. Production of acquired immunodeficiency syndrome-associated retrovirus in human and nonhumand cells transfected with an infectious molecular clone. J. Virol. 59, 284–291.

Adler, J., Parmryd, I., 2010. Quantifying colocalization by correlation: the Pearson correlation coefficient is superior to the Mander's overlap coefficient. Cytom. A. 77, 733–742.

Alfadhli, A., Mack, A., Ritchie, C., Cylinder, I., Harper, L., Tedbury, P., Freed, E.O., Barklis, E., 2016. Trimer enhancement mutation effects on HIV-1 matrix protein binding activities. J. Virol. 90, 5657–5664.

Barklis, E., Staubus, A.O., Mack, A., Harper, L., Barklis, R.L., Alfadhli, A., 2018. Lipid biosensor interactions with wild type and matrix deletion HIV-1 Gag proteins. Virology 518, 264–271.

Bernstein, H., Tucker, S., Hunter, E., Schutzbach, J., Compans, R.W., 1994. Human immunodeficiency virus type 1 envelope glycoprotein is modified by O-linked oligosaccharides. J. Virol. 68, 463–468.

Bhakta, S., Shang, L., Prince, D., Hunter, E., 2011. Mutagenesis of tyrosine and di-leucine motifs in the HIV-1 envelope cytoplasmic domain results in a loss of Env-mediated fusion and infectivity. Retrovirology 8, 37.

Bhatia, A.K., Kaushik, R., Campbell, N., Pontow, S., Ratner, L., 2009. Mutation of critical serine residues in HIV-1 matrix result in an envelope incorporation defect which can be rescued by truncation of the gp41 cytoplasmic tail. Virology 384, 233–241.

Boge, M., Wyss, S., Bonifacino, J., Thali, M., 1998. A membrane-proximal tyrosine-based signal mediates internalization of the HIV-1 envelope glycoprotein via interaction with the AP-2 clathrin adaptor. J. Biol. Chem. 273, 15773–15778.

Brizzard, B., Chubet, R., 2001. Epitope tagging of recombinant proteins. Curr. Protoc. Neurosci. https://doi.org/10.1002/0471142301.ns0508s00. (Chapter 5): Unit 5.8.

Checkley, M., Luttge, B., Freed, E.O., 2011. HIV-1 envelope protein biosynthesis, trafficking and incorporation. J. Mol. Biol. 410, 582–608.

Dorfman, T., Mammano, F., Haseltine, W., Gottlinger, H., 1994. Role of the matrix protein in the virion association of the human immunodeficiency virus type 1 envelope glycoprotein. J. Virol. 68, 1689–1696.

DuBridge, R., Tang, P., Hsia, H., Leong, P., Miller, J., Calos, M., 1987. Analysis of mutation in human cells by using an Epstein-Barr virus shuttle system. Mol. Cell. Biol. 7, 379–387.

Earl, P., Doms, R., Moss, B., 1990. Oligomeric structure of the human immunodeficiency virus type 1 envelope glycoprotein. Proc. Natl. Acad. Sci. U.S.A. 87, 648–652.

Freed, E., Martin, M., 1995. Virion incorporation of envelope glycoproteins with long but not short cytoplasmic tails is blocked by specific, single amino acid substitutions in the human immunodeficiency virus type 1 matrix. J. Virol. 69 1984–9.

Freed, E., Martin, M., 1996. Domains of the human immunodeficiency virus type 1 matrix and gp41 cytoplasmic tail required for envelope incorporation into virions. J. Virol. 70, 341–351.
Hallenberger, S., Bosch, V., Angliker, H., Shaw, E., Klenk, H., Garten, W., 1992. Inhibition of furin-mediated cleavage activation of HIV-1 glycoprotein gp160. Nature 360, 358–361.
Jiang, J., Aiken, C., 2007. Maturation-dependent human immunodeficiency virus type 1 particle fusion requires a carboxyl-terminal region of the gp41 cytoplasmic tail. J. Virol. 81, 9999–10008.
Kabat, D., Kozak, S., Wehrly, K., Chesebro, B., 1994. Differences in CD4 dependence for infectivity of laboratory-adapted and primary patient isolates of human immunodeficiency virus type 1. J. Virol. 68, 2570–2577.
Kirschman, J., Qi, M., Ding, L., Hammonds, J., Dienger-Stambaugh, K., Wang, J., Lapierre, L., Goldenring, J., Spearman, P., 2018. HIV-1 envelope glycoprotein trafficking through the endosomal recycling compartment is required for particle incorporation. J. Virol. 92 e01893-17.
Mammano, F., Kondo, E., Sodroski, J., Bukovsky, A., Gottlinger, H., 1995. Rescue of human immunodeficiency virus type 1 matrix protein mutants by envelope glycoproteins with short cytoplasmic domains. J. Virol. 69 324-3830.
Montefiori, D., Robinson, W., Mitchell, W., 1988. Role of protein N-glycosylation in pathogenesis of human immunodeficiency virus type 1. Proc. Natl. Acad. Sci. U.S.A. 85, 9248–9252.
Murakami, T., Freed, E., 2000a. The long cytoplasmic tail of gp41 is required in a cell type-dependent manner for HIV-1 envelope glycoprotein incorporation into virions. Proc. Natl. Acad. Sci. U.S.A. 97, 343–348.
Murakami, T., Freed, E., 2000b. Genetic evidence for an interaction between human immunodeficiency virus type 1 matrix and alpha-helix 2 of the gp41 cytoplasmic tail. J. Virol. 74, 3548–3554.
Murphy, R.E., Samal, A.B., Vlach, J., Saad, J., 2017. Solution structure and membrane interaction of the cytoplasmic tail of HIV-1 gp41 protein. Structure 25, 1708–1718.
Ohno, H., Aguilar, R., Fournier, M., Hennecke, S., Cosson, P., Bonifacino, J., 1997. Interaction of endocytic signals from the HIV-1 envelope glycoprotein complex with members of the adaptor medium chain family. Virology 238, 305–315.
Pinter, A., Honnen, W., Tilley, S., Bona, C., Zaghouani, H., Gorny, M., Zolla-Pazner, S., 1989. Oligomeric structure of gp41, the transmembrane protein of human immunodeficiency virus type 1. J. Virol. 63, 2674–2679.
Qi, M., Williams, J., Chu, H., Chen, X., Wang, J., Ding, L., Akhirome, E., Wen, X., Lapierre, L., Goldenring, J., Spearman, P., 2013. Rab11-FIP1C and Rab14 direct plasma membrane sorting and particle incorporation of the HIV-1 envelope glycoprotein complex. PLoS Pathog. 9 (4), e1003278.
Qi, M., Chu, H., Chen, X., Choi, J., Wen, X., Hammonds, J., Ding, L., Hunter, E., Spearman, E., 2015. A tyrosine-based motif in the HIV-1 envelope glycoprotein tail mediates cell-type- and Rab11-FIP1C-dependent incorporation into virions. Proc. Natl. Acad. Sci. U.S.A. 112, 7575–7580.
Reil, H., Bukovsky, A., Gelderblom, H., Gottlinger, H., 1998. Efficient HIV-1 replication can occur in the absence of the viral matrix protein. EMBO J. 17, 2699–2708.
Ritchie, C., Cylinder, I., Platt, E., Barklis, E., 2015. Analysis of HIV-1 Gag protein interactions via biotin ligase tagging. J. Virol. 89, 3988–4001.
Roux, K., Kim, D., Raida, M., Burke, B., 2012. A promiscuous biotin ligase fusion protein identifies proximal and interacting proteins in mammalian cells. J. Cell Biol. 196, 801–810.
Schawaller, M., Smith, G., Skehel, J., Wiley, D., 1989. Studies with crosslinking reagents on the oligomeric structure of the env glycoprotein of HIV. Virology 172, 367–369.
Scherer, W., Syverton, J., Gey, G.O., 1953. Studies on the propagation in vitro of poliomyelitis viruses. IV. Viral multiplication in a stable strain of human malignant epithelial (strain HeLa) derived from an epidermoid carcinoma of the cervix. J. Exp. Med. 97, 695–710.
Schneider, C., Rasband, W., Eliceiri, K., 2012. NIH Image to ImageJ: 25 years of image analysis. Nat. Methods 9, 671–675.
Tedbury, P., Ablan, S., Freed, E., 2013. Global rescue of defects in HIV-1 envelope glycoprotein incorporation: implications for matrix structure. PLoS Pathog. 9 (11), e1003739.
Tedbury, P., Novikova, M., Ablan, S., Freed, E., 2016. Biochemical evidence of a role for matrix trimerization in HIV-1 envelope glycoprotein incorporation. Proc. Natl. Acad. Sci. U.S.A. 113, E182–E190.
Turner, J., Lencer, W., Carlson, S., Madara, J., 1996. Carboxyl-terminal vesicular stomatitus virus G protein-tagged intestinal Na+-dependent glucose cotransporter (SGLT1). J. Biol. Chem. 271, 7738–7744.
Waheed, A., Ablan, S., Mankowski, M., Cummins, J., Ptak, R., Schaffner, C., Freed, E., 2006. Inhibition of HIV-1 replication by amphotericin B methyl ester: selection for resistant variants. J. Biol. Chem. 281, 28699–28711.
Waheed, A., Ablan, S., Roser, J., Sowder, R., Schaffner, C., Chertova, E., Freed, E., 2007. HIV-1 escape from the entry-inhibiting effects of a cholesterol-binding compound via cleavage of gp41 by the viral protease. Proc. Natl. Acad. Sci. U.S.A. 104, 8467–8471.
Wang, C.-T., Zhang, Y., McDermott, J., Barklis, E., 1993. Conditional infectivity of a human immunodeficiency virus matrix domain deletion mutant. J. Virol. 67, 7067–7076.
Wyss, S., Berlioz-Torrent, C., Boge, M., Blot, G., Höning, S., Benarous, R., Thali, M., 2001. The highly conserved C-terminal dileucine motif in the cytosolic domain of the human immunodeficiency virus type 1 envelope glycoprotein is critical for its association with the AP-1 clathrin adaptor. J. Virol. 75, 2982–2992.
Yu, X., Yuan, X., Matsuda, Z., Lee, T., Essex, M., 1992. The matrix protein of human immunodeficiency virus type 1 is required for incorporation of viral envelope protein into mature virions. J. Virol. 66, 4966–4971.
Zhang, G., Gurtu, V., Kain, S., 1996. An enhanced green fluorescent protein allows sensitive detection of gene transfer in mammalian cells. Biochem. Biophys. Res. Commun. 227, 707–711.